

Article citation info:

Jiang Y, Lu Z, A Feature Extraction Method for Parameter Fault Diagnosis of DC-DC Converters Under Strong Noise and Small Sample Conditions, *Eksploracja i Niezawodność – Maintenance and Reliability* 2026; 28(1) <http://doi.org/10.17531/ein/207882>

## A Feature Extraction Method for Parameter Fault Diagnosis of DC-DC Converters Under Strong Noise and Small Sample Conditions

Indexed by:



Yuanyuan Jiang<sup>a</sup>, Zhou Lu<sup>a,\*</sup>

<sup>a</sup> Anhui University of Science and Technology, China

### Highlights

- It is especially effective in strong noise and small sample scenarios.
- AEDFE uses a simple convolutional neural network (CNN) for implementation.
- It achieves 100% diagnostic accuracy in noisy environments.
- AEDFE demonstrates superior performance under complex conditions.

### Abstract

Parametric fault diagnosis of DC-DC converters faces significant challenges under strong noise and small sample conditions due to the low accuracy of existing feature extraction methods. To address this problem, we propose an Adaptive Euler Difference Feature Extraction (AEDFE) method, which effectively captures spatial features from fault signals to enhance the distinction between faults of varying severities. This method is implemented via a lightweight convolutional neural network, enabling accurate fault classification even under adverse conditions. Experimental results show that the proposed AEDFE achieves 100% diagnostic accuracy in strong noise environments, outperforming three existing methods by an average margin of 61.61%. Furthermore, when the training data is reduced to 10% of the original, AEDFE still maintains an accuracy of 99.98%, representing a 77.64% improvement in diagnostic precision over the comparative models. These results highlight the robustness and effectiveness of AEDFE in noisy and data-scarce scenarios.

### Keywords

DC-DC converter, parametric fault diagnosis, strong noise, small sample, 1DCNN

This is an open access article under the CC BY license (<https://creativecommons.org/licenses/by/4.0/>)

### 1. Introduction

With the rapid development of integrated circuit technology and computer technology, the internal structures and manufacturing scales of electronic circuit systems and equipment have become increasingly large and complex. Among these, DC-DC circuits play a crucial role as an integral part of electronic circuit systems, quickly integrating into people's lives, work, and economic development. They are essential in various fields, including communication systems, transportation, medical devices, industrial production, and even national defense and aerospace. DC-DC circuits have become a vital pillar for ensuring people's well-being, maintaining national security, and

promoting the advancement of national technology [1-3].

DC-DC circuit failures can be primarily classified into two types: structural failures [4] (hard failures) and parametric failures [5] (soft failures). Structural failures have been the focus of numerous research methods [6-7], making detection relatively straightforward. However, when structural failures occur, they can lead to severe circuit failures or even total breakdowns, resulting in significant losses. Additionally, diagnosing hard failures is typically a post-failure remedy; once the fault has occurred, the damage is already done. Before hard failures arise, parametric failures often occur due to the gradual

(\*) Corresponding author.  
E-mail addresses:

Y. Jiang, (ORCID: 0000-0001-6167-543X) [jyyLL672@163.com](mailto:jyyLL672@163.com), Z. Lu (ORCID: 0009-0006-1612-2901) [zlu23567@gmail.com](mailto:zlu23567@gmail.com)

degradation of component parameters. The early signs of parametric failures manifest as a decline in circuit performance, leading to abnormal device operation [8]. However, the early characteristics of parametric failures are subtle and often go unnoticed. If these failures are allowed to persist, the degradation of component parameters may reach a critical point, resulting in structural failures with serious consequences. Therefore, timely assessment of the health status of DC-DC circuits in the presence of parametric failures is crucial for ensuring their reliability and achieving accurate, rapid fault diagnosis.

DC-DC converters are widely used to provide various supply voltages for electronic components on circuit boards. However, as switching frequencies increase, switching noise also rises [9]. This not only interferes with the circuit's switching frequency, regulation accuracy, and stability, but it also leads to output voltage fluctuations, impacting the overall performance of the circuit and the reliability of the equipment. In high-noise environments, this noise interference can obscure the early signs of parametric failures, making detection and diagnosis more challenging [10]. Due to the subtle nature of failure characteristics and their susceptibility to noise interference, obtaining sufficient high-quality samples becomes challenging. This limitation restricts the model's ability to learn failure patterns, reduces detection sensitivity, and increases the risk of overfitting. Consequently, the issue of small sample data is particularly pronounced in fault diagnosis [11]. To ensure effective health monitoring and fault diagnosis of DC-DC circuits in complex environments, it is essential to adopt robust methodologies that facilitate rapid and accurate diagnostics.

With the rapid development of computer technology, machine learning-based methods are quickly becoming one of the mainstream approaches for fault diagnosis in electronic circuits [12]. The methods for diagnosing faults in DC-DC circuits primarily involve two key techniques: fault feature extraction and fault classification. Jiang et al. [13] utilized empirical mode decomposition (EMD) to decompose light rail noise signals, extracting the energy and kurtosis features of the intrinsic mode functions (IMFs) to obtain multi-scale kurtosis features, which were then input into a neural network to identify wheel-rail fault types. Li Rui et al. [14] applied complete ensemble empirical mode decomposition with adaptive noise

(CEEMDAN) to adaptively decompose the vibration signals of one-way valves in high-pressure diaphragm pumps into multiple intrinsic mode functions (IMFs). They then calculated multi-scale permutation entropy values to extract signal features and ultimately established a fault diagnosis model. Sudhar et al. [15] addressed noise issues in input signals through variational mode decomposition (VMD) and then performed principal component analysis (PCA) for dimensionality reduction, thereby improving the accuracy of fault loss predictions. Common classifiers include BP neural networks [16], various optimized support vector machines (SVM) [17-18], and extreme learning machines (ELM) [19]. However, traditional machine learning methods often struggle with signal processing, as most classifiers are shallow network models, which limits their effectiveness [20]. While traditional feature extraction methods can mitigate signal noise to some extent, their diagnostic performance often deteriorates significantly in complex or high-noise environments. Moreover, these methods generally require large amounts of labeled data for training, making them less effective in small-sample scenarios commonly encountered in practical applications. This reliance limits their generalization ability and robustness when data is scarce or noisy. To overcome these challenges, this paper proposes an improved feature extraction method designed to enhance both the accuracy and practical applicability of fault diagnosis under noisy and limited-data conditions.

In real-world applications, DC-DC converters often operate under strong electromagnetic interference and limited data availability, making the diagnosis of parametric faults—caused by subtle component degradations—particularly challenging. Traditional feature extraction methods typically focus on decomposing signal components to suppress noise and isolate relevant features. While effective in general cases, they struggle to distinguish slight differences in fault severity, especially under high-noise conditions, leading to reduced diagnostic accuracy. To address this issue, we propose a novel method called Adaptive Eulerian Difference Feature Extraction (AEDFE), which leverages the spatial information embedded in fault signals. Unlike conventional approaches, AEDFE enhances the representation of spatial features rather than relying solely on signal decomposition, significantly improving the model's ability to differentiate between faults of varying

severity. The extracted features are more robust and discriminative, enabling high-accuracy diagnosis even in noisy and data-scarce environments, thus offering strong practical value for real-world fault diagnosis scenarios. First, we apply AEDFE to process the collected voltage signals, effectively extracting the spatial features and indirectly achieving noise suppression. The processed features are then used as inputs for a convolutional neural network (CNN), facilitating precise diagnosis of parametric faults in DC-DC converters. The fault diagnosis workflow for DC-DC circuits, illustrated in Fig.1, combines AEDFE with a one-dimensional convolutional neural network (1DCNN).

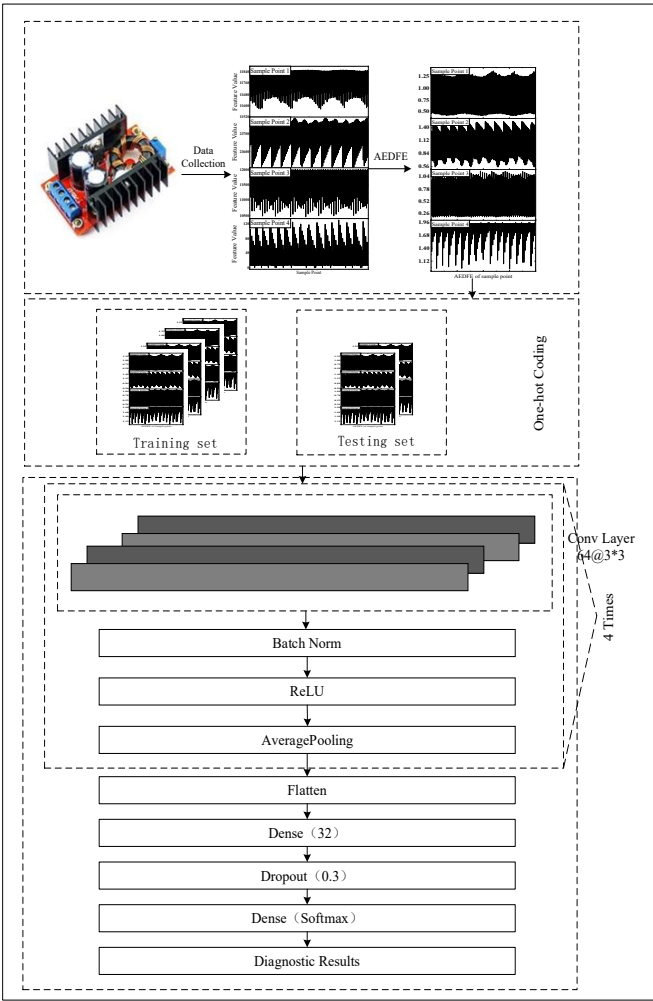


Fig. 1. Fault Diagnosis Workflow for DC-DC Circuits.

Initially, AEDFE is used to extract features from the voltage data related to parametric faults in the DC-DC converter. Subsequently, the extracted features are divided into training and testing sets in a 70:30 ratio to construct the fault dataset, which serves as input data for the 1DCNN, ultimately enabling accurate diagnosis of parametric faults in the DC-DC converter.

The innovative contributions of this work are summarized as follows:

1) This study proposes an innovative AEDFE method for effectively extracting spatial features from the voltage signals of DC-DC converters, overcoming the challenges of traditional methods in feature extraction under strong noise environments.

2) The AEDFE method significantly enhances the ability to extract features of parametric faults of varying degrees by leveraging the spatial information of the signals, allowing for effective utilization and accurate identification of fault characteristics even in high-noise conditions.

3) By combining the AEDFE method with a 1DCNN, an efficient fault diagnosis process is established. This combined approach enables high-precision fault diagnosis in small sample environments, improving the accuracy and practicality of the model.

## 2. AEDFE

In small sample fault diagnosis under strong noise environments, the primary challenge lies in extracting effective fault features from data affected by noise interference. Noise obscures the true fault information, making it difficult to identify distinct features. Additionally, the small sample issue complicates the training of high-accuracy models, as the limited amount of data can lead to overfitting, adversely affecting the model's generalization ability. Therefore, there is an urgent need for an innovative approach in the field of fault diagnosis that can effectively extract fault features under conditions of strong noise and data scarcity. This method should ensure model accuracy to enhance the performance of diagnostic systems and the reliability of equipment.

Euler's formula in complex analysis is expressed as:

$$e^{ix} = \cos(x) + i \sin(x) \quad (1)$$

This signifies that both sides of the equation are proven to hold true in the complex domain, implying that the equality

$$e^{ix} - (\cos(x) + i \sin(x)) = 0 \quad (2)$$

is valid in the complex plane. This article proposes the transfer of Euler's identity in the complex domain to Cartesian coordinates and introduces the AEDFE method. By applying a differential approach to Euler's identity, the aim is to analyze data more deeply and capture spatial features within the signals. This method employs a multi-step mathematical transformation

process that incorporates data scaling, trigonometric transformations, exponential transformations, and feature differentiation, effectively extracting potential complex features from the data. First, data is standardized and scaled to the interval  $[0, 1]$  to eliminate dimensional influences and provide a consistent scale for subsequent transformations. Next, the inverse cosine function is utilized to convert the standardized data into angles, introducing periodic features and nonlinear information. Following this, an exponential function is applied to the product of the angles and standardized data, generating feature values with higher nonlinear characteristics. Finally, the absolute differences between features generated from trigonometric and exponential transformations are computed, and these differences are adjusted for their mean to highlight meaningful feature distinctions in the data. Through this comprehensive approach, not only is the ability to capture spatial features in signals enhanced, but the expressiveness of the data features is also improved, laying a solid foundation for further analysis and modeling.

The specific steps of AEDFE are as follows:

#### 1) Data Scaling

To ensure that different features have the same scale and eliminate the dimensional influence between the data, the original data is first standardized. Let the original data column be  $x$ , and its standardization formula is:

$$x_i = \frac{x - \min(x)}{\max(x) - \min(x)} \quad (3)$$

where  $x_i$  represents the standardized data value, and  $\min(x)$  and  $\max(x)$  are the minimum and maximum values in the data column, respectively. Using this formula, the data is linearly scaled to the range  $[0, 1]$ , ensuring that all data points are within a uniform scale.

#### 2) Calculate the Arc Cosine Value

After standardization, the next step is to calculate the arc cosine values of the standardized data to obtain the corresponding angles. This process can be expressed as:

$$\phi = \arccos(x_i) \quad (4)$$

where  $\phi$  is the arc cosine angle corresponding to the standardized data  $x_i$ . The arc cosine function  $\arccos$  maps the standardized data to angles in the range  $[0, \pi]$ . This step introduces a nonlinear transformation, effectively capturing the periodic characteristics of the data.

#### 3) Feature Calculation

Based on the transformation using Euler's formula, this paper defines two new features that combine the nonlinear effects of trigonometric functions and exponential functions:

(1) First Feature Value:

$$Euler\_Feature\_1 = \cos(\phi) + x_i \sin(\phi) \quad (5)$$

This feature integrates the cosine value of the angle with the product of the sine value and standardized data. This combination effectively captures periodic and nonlinear patterns in the data through the interplay of the two trigonometric functions.

(2) Second Feature Value:

$$Euler\_Feature\_2 = \exp(x_i \phi) \quad (6)$$

This feature performs a nonlinear expansion using the exponential function  $\exp$  on the product of the standardized data  $x_i$  and the angle  $\phi$ . The second feature value effectively highlights the nonlinear relationships in the data, making the complex patterns more prominent.

#### 4) Calculate AEDFE

To extract meaningful features from the data, the absolute differences between the first and second feature values are calculated, followed by mean adjustment of these differences. The specific steps are as follows:

(1) Calculate the Absolute Differences:

$$D_i = |Euler\_Feature\_1 - Euler\_Feature\_2| \quad (7)$$

where  $D_i$  represents the absolute difference between the first and second feature values.

(2) Mean Adjustment:

To remove the offset in the differences, the mean of all differences needs to be calculated and subtracted from each difference.

$$mean_D = \frac{1}{n} \sum_{i=1}^n D_i \quad (8)$$

$$AEDFE_i = D_i - mean_D \quad (9)$$

Here,  $n$  is the total number of data points, and  $mean_D$  is the mean of all differences. This mean adjustment makes the final feature  $AEDFE_i$  more centralized, enhancing its stability in data analysis.

The proposed method generates a novel feature, Adaptive Eulerian Difference Feature Extraction (AEDFE), through a series of mathematical transformations including normalization, angle calculation, nonlinear mapping, and

feature differentiation. By integrating the nonlinear characteristics of trigonometric and exponential functions, AEDFE is able to capture complex data patterns and reveal underlying structural information that traditional linear methods may overlook. This innovative approach offers a fresh perspective for feature extraction from one-dimensional signals,

Table 1. mathematical formul.

Step	mathematical formula	variable definitions
1) Data Scaling	$x_i = \frac{x - \min(x)}{\max(x) - \min(x)}$	$x_i$ :standardized data; $\min(x) / \max(x)$ :maximum/minimum of the column;scales data to [0, 1]
2) Calculate the Arc Cosine Value	$\phi = \arccos(x_i)$	$\phi$ :arccos angle of standardized data $x_i$ ; nonlinear mapping to capture periodicity; $x_i$ :standardized input data (range-scaled to [0, $\pi$ ])
3) Feature Calculation		
(1) First Feature Value:	$Euler\_Feature\_1 = \cos(\phi) + x_i \sin(\phi)$	First Feature: combines $\cos(\text{angle})$ and $\sin(\text{angle}) \times \text{data}$ to capture nonlinear and periodic patterns.
(2) Second Feature Value:	$Euler\_Feature\_2 = \exp(x_i \phi)$	Second Feature: applies $\exp(x \times a)$ to highlight nonlinear relationships and complex patterns.
4) Calculate AEDFE		
(1) Calculate the Absolute Differences:	$D_i =  Euler\_Feature\_1 - Euler\_Feature\_2 $	$D_i$ :absolute difference between the First Feature and Second Feature
(2) Mean Adjustment:	$mean_D = \frac{1}{n} \sum_{i=1}^n D_i$ $AEDFE_i = D_i - mean_D$	$n$ :number of data points; $mean_D$ :average of differences, used to center AEDFE.

### 3. 1D Convolutional Neural Networks

#### 3.1. Introduction to 1D Convolutional Neural Networks

1DCNN are a type of multi-layer feedforward neural network, typically consisting of three basic components: convolutional layers, pooling layers, and fully connected layers. In 1DCNNs, convolutional layers extract features from the input data through convolution operations, while pooling layers further reduce the size of the feature maps through downsampling, thereby decreasing computational complexity. Finally, the fully connected layers use the extracted features to perform classification or regression tasks, with a structure and computational method similar to traditional feedforward neural networks.

##### 1) Convolutional Layer

The convolutional layer learns features from the input data through convolution calculations. It consists of multiple feature maps, with each neuron in a feature map connected to a local

effectively enhancing the representational capacity of the data for subsequent analysis and model training. Furthermore, the nonlinear transformations contribute to improved robustness against noise and better adaptability in small-sample scenarios, thereby increasing the practical applicability of the model.

region of the previous layer's feature map via a convolutional kernel (weight set), known as the receptive field. After the convolution operation, the results pass through a nonlinear activation function to generate the feature maps for the next layer. Different convolutional kernels produce different feature maps, and each feature map is computed using the same convolutional kernel. This weight sharing technique reduces model complexity and simplifies the training process [21]. The forward propagation of a convolutional neural network can be represented by the following formula:

$$y_t = ReLU(\sum_{k=0}^{K-1} (x_{t+k} \omega_k) + b) \quad (10)$$

Here,  $x_{t+k}$  is the value of the input data at position  $t + k$ ,  $\omega_k$  is the weight of the convolutional kernel at position  $k$ ,  $b$  is the bias term, and  $ReLU$  is the activation function.

##### 2) Pooling Layer

In convolutional neural networks, pooling layers are typically inserted between consecutive convolutional layers to gradually reduce the dimensions of the output from the convolutional

layers. This helps decrease the number of parameters and the computational load, mitigate overfitting, and perform secondary feature extraction. The pooling layer keeps the number of feature maps unchanged, with the most commonly used methods being max pooling and average pooling [22]. In this paper, average pooling is adopted because it better preserves the global information of features and results in more stable training compared to max pooling. The calculation formula is as follows:

$$y_t = \frac{1}{k} \sum_{i=0}^{k-1} x_{t+i} \quad (11)$$

Here,  $k$  is the size of the pooling window.

### 3) Activation layer

Activation functions are typically used to perform nonlinear transformations on the outputs of convolutional computations to obtain nonlinear representations of the input data, thereby enhancing the network's feature learning capability [23]. A commonly used activation function in CNNs is the ReLU function, which is defined as:

$$\text{ReLU}(x) = \max(0, x) \quad (12)$$

### 4) Fully connected layer

The fully connected layer is typically located at the end of a convolutional neural network, mapping the features extracted by the convolutional and pooling layers to the final classification results. In the fully connected layer, the softmax function is used to convert the network's raw output into a probability distribution for classification tasks [24]. Its formula is as follows:

$$p_i = \frac{e^{z_i}}{\sum_{j=1}^K e^{z_j}} \quad (13)$$

Here,  $Z_j$  is the  $i$ -th component of vector  $Z$ , and  $\sum_{j=1}^K e^{z_j}$  is the sum of the exponential values of all class scores, used for normalization to ensure that the sum of all probability values equals 1.

In this study, the key hyperparameters of the 1D-CNN model, including the convolution kernel size, number of kernels, dropout rate, and learning rate, were reasonably determined based on a review of relevant literature and extensive preliminary experiments. Specifically, a kernel size of 3 was chosen to effectively capture local details in the input time series, while the stacking of multiple convolutional layers enabled the model to learn long-term dependencies. The number of kernels was set to 64 to balance model expressiveness and

computational complexity, thereby avoiding overfitting caused by an excessively large model. A dropout rate of 0.3 was selected, which was demonstrated through experiments to effectively suppress overfitting and improve the model's generalization ability. The learning rate was set to 0.0001 to ensure stable convergence during training and to prevent training oscillations or divergence that could occur with a higher learning rate.

## 3.2. 1D CNN Fault Diagnosis Model

The 1DCNN fault diagnosis model is established in three steps:

1) Data preprocessing: We first add Gaussian white noise to the original data to simulate the noise impact in daily industrial production. Next, we use feature extraction methods to extract features from the data with added noise. After feature extraction, we divide the feature data into a dataset and split it into training and testing sets according to a predetermined ratio.

2) Model training: We selected the Adam optimizer and cross-entropy loss function. The Adam optimizer is widely used due to its ease of implementation, high computational efficiency, and low memory requirements. Compared to SGD and RMSprop, Adam typically demonstrates superior optimization performance. The cross-entropy loss function was chosen for its strong robustness in handling noise, making it suitable for high-noise environments. We set the learning rate to 0.0001 to achieve a good balance between training speed and model convergence.

3) Model testing: We evaluate the model using the testing set. Performance testing on the testing set allows us to understand the model's performance on actual data and comprehensively assess its classification effectiveness.

## 4. DC-DC Boost Converter Fault Data

### 4.1. Experimental Subjects

To verify the performance of the circuit fault feature extraction diagnostic model, a 150W boost converter controlled by the UC3843 chip is tested as an example. The input voltage of the circuit is 12V, the output voltage is 24V, and the load is 100  $\Omega$  with a resistor power of 50W. The standard values for capacitors C1 and C5 are both 1000 $\mu$ F. The circuit schematic, parameter fault testing platform, and physical diagram of the circuit are shown in Fig.2, Fig.3, and Fig.4, respectively. The basic information of the circuit is provided in Table 2.

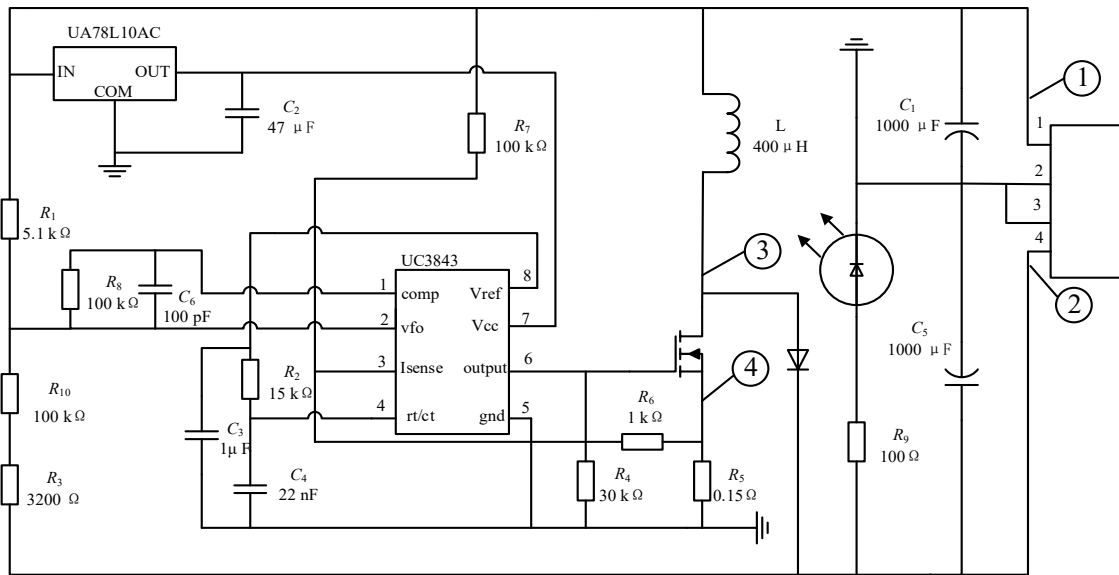


Fig. 2. 150W DC-DC Boost Converter Circuit Schematic.

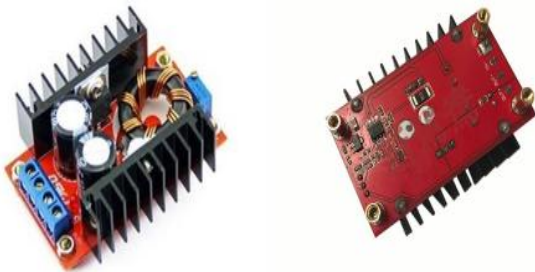


Fig. 3. 150W DC-DC Boost Converter Actual Circuit Diagram.

Table 2. Basic Information of 150W DC-DC Boost Converter Circuit.

Circuit Type	150W DC-DC Boost Converter Circuit
Input Voltage	10-32V
Output Voltage	12-35V
Input Current	10A(MAX)
Output Current	6A(MAX)

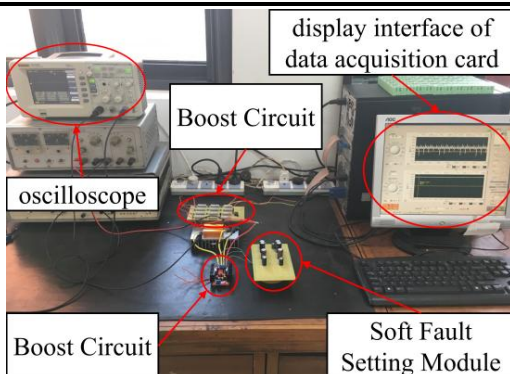


Fig. 4. Parameter Fault Platform of 150W DC-DC Boost Converter Circuit.

#### 4.2. Experimental Data

In this paper, the electrolytic capacitors C1 and C5 in the 150W

DC-DC Boost Converter circuit are selected. In the actual circuit, a capacitor degradation of 0-10% is considered normal, so a range of 10%-50% degradation is divided into 15 fault modes. The fault setting modes are shown in Table 3. Among them, f11 represents the normal mode, f12, f13, and f14 represent soft faults of C1, while f21, f31, and f41 represent soft faults of C5. The remaining fault modes are dual soft faults of both C1 and C5.

Table 3. Fault Mode Settings for 150W DC-DC Boost Converter Circuit Parameters

Failure Mode	C1/C5(μF)	C1/C5 Degradation Level (%)	Label
F11	988/916	0~10/0~10	1
F12	988/887	0~10/10~20	2
F13	988/653	0~10/30~40	3
F14	988/554	0~10/40~50	4
F21	864/916	10~20/0~10	5
F22	864/887	10~20/10~20	6
F23	864/653	10~20/30~40	7
F24	864/554	10~20/40~50	8
F31	655/916	30~40/0~10	9
F32	655/887	30~40/10~20	10
F33	655/653	30~40/30~40	11
F34	655/554	30~40/40~50	12
F41	546/916	40~50/0~10	13
F42	546/887	40~50/10~20	14
F43	546/653	40~50/30~40	15
F44	546/554	40~50/40~50	16

To ensure that the collected DC-DC circuit voltage signals adequately capture the fault information of C1 and C5, this paper analyzes the voltage signals from four measurement points as shown in Schematic Diagram 2. Each measurement point has 2,000 sampling points, with 50 samples taken for each fault state, and each sampling duration is 0.5 seconds. The voltage signals obtained from the four measurement points can accurately represent the degradation state of the circuit. Fig.5 illustrates the voltage waveforms from the four measurement points under the F43 fault mode.

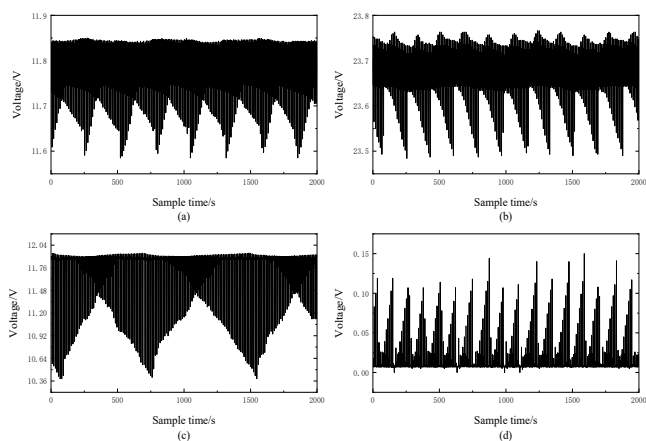


Fig. 5. Voltage Signals: (a) Input Voltage Signal; (b) Output Voltage Waveform; (c) MOSFET Drain Voltage; (d) MOSFET Source Voltage.

### 4.3. Comparison of Fault Data Processing Results

To visually demonstrate the capability of AEDFE in extracting fault features, we take the data from Measurement Point 1 for Fault Mode 15 (F43) as an example. The polar plots, or radar charts, processed by different feature extraction algorithms are presented in Fig.6 to Fig.10. The radar chart provides an intuitive representation of multidimensional data, allowing multiple variables to be compared within the same graph. It showcases the multidimensional characteristics of the data, helps identify patterns and anomalies, and evaluates the effectiveness of different feature extraction methods, while clearly displaying the overall distribution and periodic changes of the data. Fig. 6 shows the radar chart for the raw data, while Fig.7 to Fig.9 present the radar charts for the data after feature extraction using traditional methods. Fig.10 displays the radar chart for the data after feature extraction using AEDFE.

From Fig.6 to Fig.9, it is evident that the spatial features in

the data extracted using traditional methods are quite chaotic, making it difficult for the model to capture and utilize this information effectively. However, as shown in Fig.10, after extraction using AEDFE, the spatial features of the data transition from chaotic to structured, demonstrating the effectiveness of AEDFE in mining and clarifying the spatial characteristics of the data.

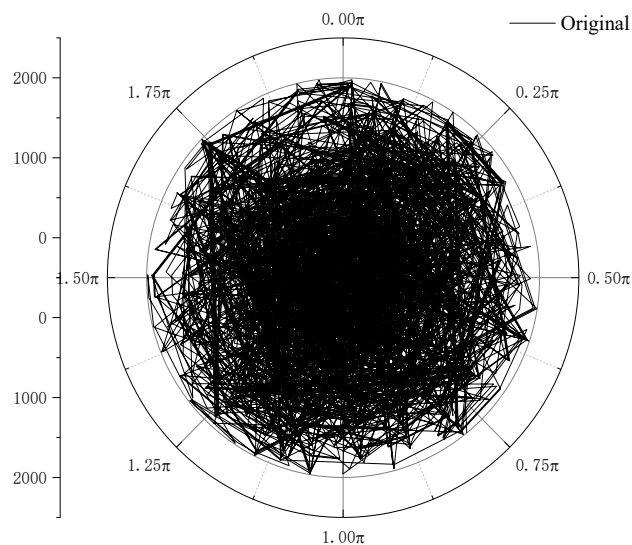


Fig. 6. Radar Chart of Raw Data

As shown in Figure 6, the features of the raw, unprocessed data are highly disordered in the spatial distribution.

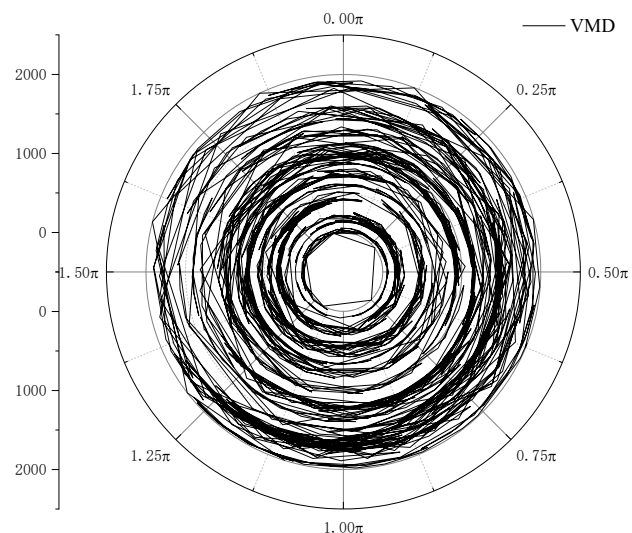


Fig. 7. Radar Chart of VMD

As shown in Figure 7, the data processed by VMD exhibits slightly clearer spatial features, but the characteristics remain indistinct and relatively disordered.

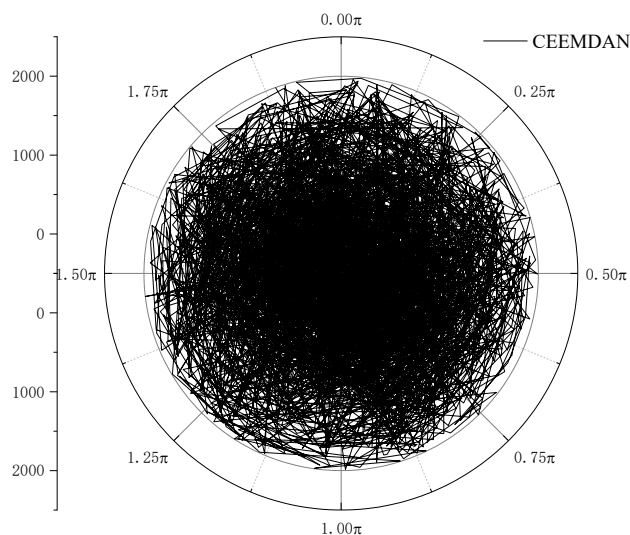


Fig. 8. Radar Chart of CEEMDAN

As shown in Figure 8, the data processed by CEEMDAN lacks a clear distribution pattern in the spatial dimension, exhibiting strong randomness.

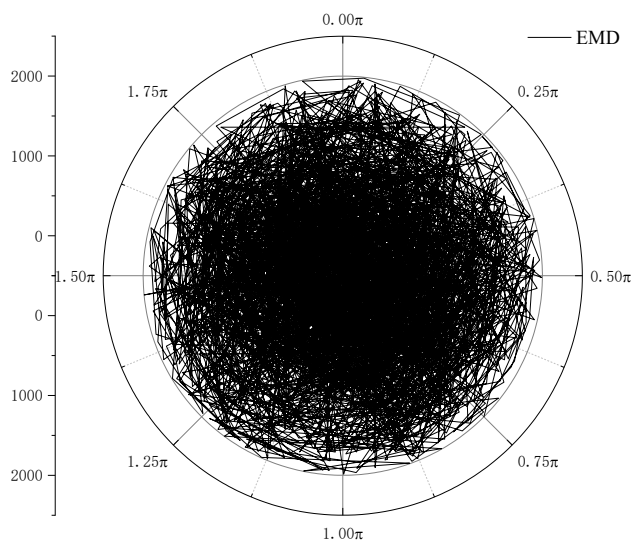


Fig. 9 Radar Chart of EMD

As shown in Figure 9, the data processed by EMD still lacks a clear distribution pattern in the spatial dimension and exhibits strong randomness.

As shown in Figure 10, the data processed by AEDFE forms a distinct feature convergence region in the radar chart, with a more consistent distribution, demonstrating clear feature centralization and distinguishability.

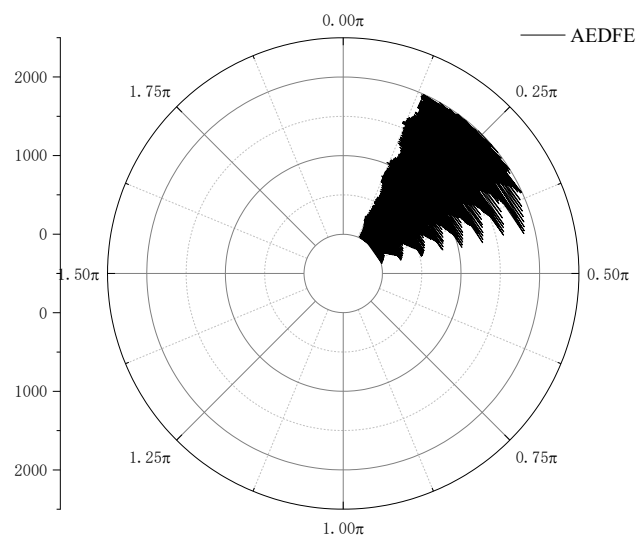


Fig. 10. Radar Chart of AEDFE.

## 5. Analysis of Experimental Results

This paper validates the proposed diagnostic method using the fault data from the DC-DC boost circuit described above. The testing software environment is Windows 10 64-bit, equipped with 32 GB of RAM, and the experiments are conducted on the PyCharm platform using the PyTorch framework. The hardware environment includes an Intel® I5-12400 CPU and a 4060 Ti 8 GB GPU. The 1D CNN used employs Cross Entropy as the loss function, Adam as the optimizer, and a learning rate of 0.0001. Each experiment involves 100 training epochs on both the training and testing datasets.

In practical working conditions, data collection is often affected by noise, which may obscure fault characteristics and make it difficult for diagnostic models to effectively extract them. Therefore, Gaussian white noise of varying magnitudes was added to the original fault data to simulate the noise environment encountered in daily production. Subsequently, the fault data was processed using feature extraction methods such as AEDFE, CEEMDAN, VMD, and EMD. In the comparative experiments, the CEEMDAN method decomposes multiple time series data files, with the parameter set to perform one screening per scale to improve computational efficiency. The first four intrinsic mode functions (IMFs) from the decomposition results are extracted for subsequent analysis, ensuring effective extraction and processing of the main signal features under noisy conditions. EMD decomposes single-channel time series data, with a key parameter set to 3, limiting

the extraction to a maximum of three IMFs. The decomposition results are saved row-wise for convenient subsequent analysis. This parameter setting helps control the decomposition levels, avoiding over-decomposition while extracting the primary signal features. VMD decomposes multi-channel data from multiple CSV files with the following key parameters: balancing factor  $\alpha = 2048$  controlling the bandwidth of decomposition, noise tolerance  $\tau = 0$ , number of modes  $K = 4$ , DC component off ( $DC = 0$ ), initialization method  $init = 1$ , and convergence tolerance  $tol = 1e-6$ . VMD decomposition is performed on each input file, outputting four IMFs which are saved separately, ensuring effective extraction of multi-scale features from the signals.

The processed data was then input into a 1D CNN for diagnosis, with each capture consisting of 2000 data points and moving the capture frame forward by 100 sampling points each time. The generated samples were randomly divided into training and testing sets in a certain proportion. The final diagnostic results of the different feature extraction methods are shown in Fig.11 to Fig.13.

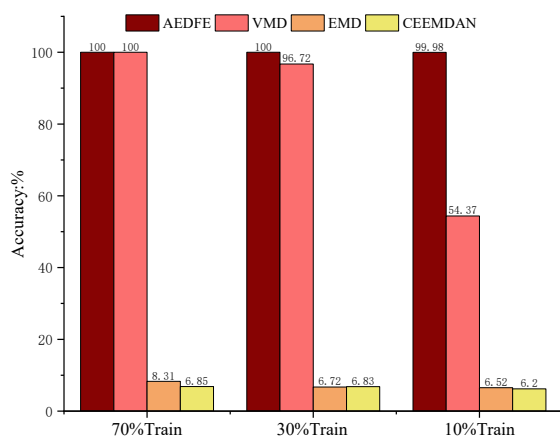


Fig. 11. Experimental results with -18 dB noise.

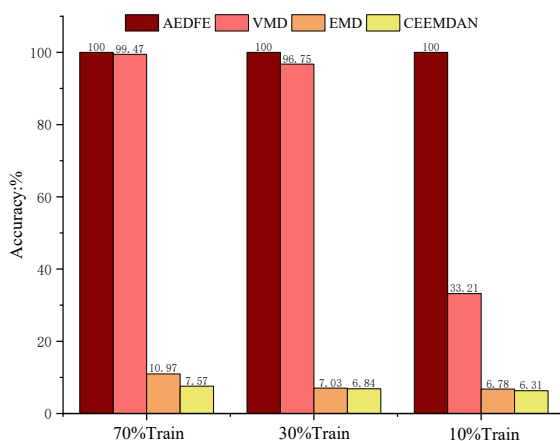


Fig. 12. Experimental results with -12 dB noise.

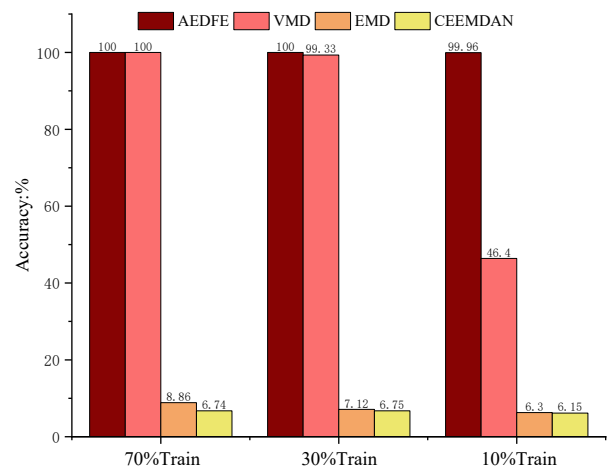


Fig. 13. Experimental results with -6 dB noise.

From the bar comparison chart in Fig.11, it can be observed that the diagnostic model using the AEDFE method achieves an accuracy of 100%, which is an increase of 61.61% compared to the average accuracy of the other three feature extraction methods. Even when the training data is reduced to 30%, this method still maintains a diagnostic accuracy of 100%, showing an average improvement of 63.24% over the other methods. Furthermore, when using only 10% of the data for training, the accuracy reaches 99.98%, with an average improvement of 77.64% compared to other methods. Fig.12 and Fig.13 also indicate improvements when -12 dB and -6 dB noise are added, respectively, compared to the other three methods. These results demonstrate that the AEDFE method excels in diagnosing DC-DC circuit parameter faults under noisy conditions and maintains efficient feature extraction performance even with a limited sample size.

Fig.14 to Fig.19 display the training processes of the AEDFE method and three comparison methods. As shown in Fig.14, Fig.16, and Fig.18, the diagnostic model trained with features generated by AEDFE achieved rapid convergence, reaching a testing diagnostic accuracy of 99.98%. In contrast, while the three comparison methods attained high training accuracy on the training data, their diagnostic accuracy on the test set was relatively low, with significant testing loss and difficulty achieving good fitting results.

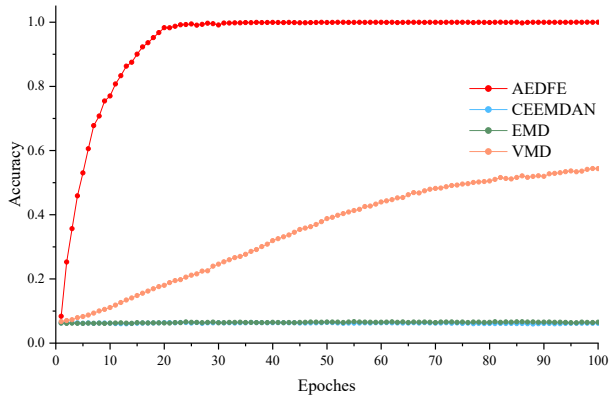


Fig. 14. Test accuracy plot of the model during the training process with 10% of the data as input for the four different methods.

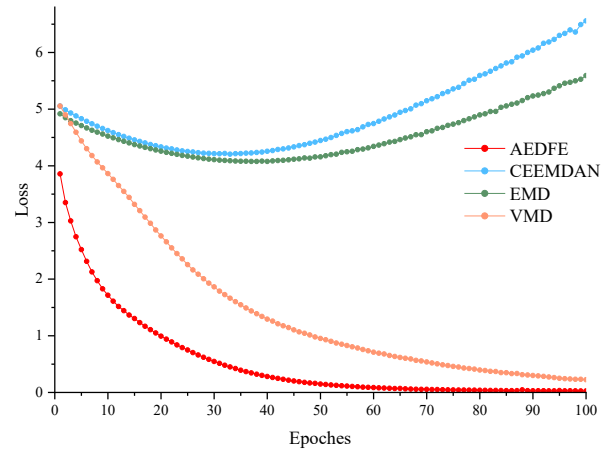


Fig. 17. Test loss plot of the model during the training process with 30% of the data as input for the four different methods.

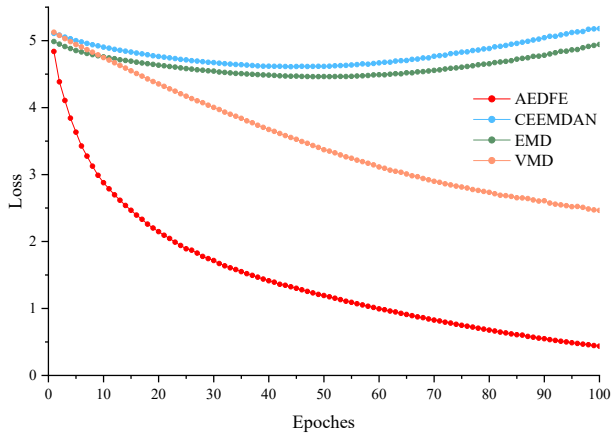


Fig. 15. Test loss plot of the model during the training process with 10% of the data as input for the four different methods.

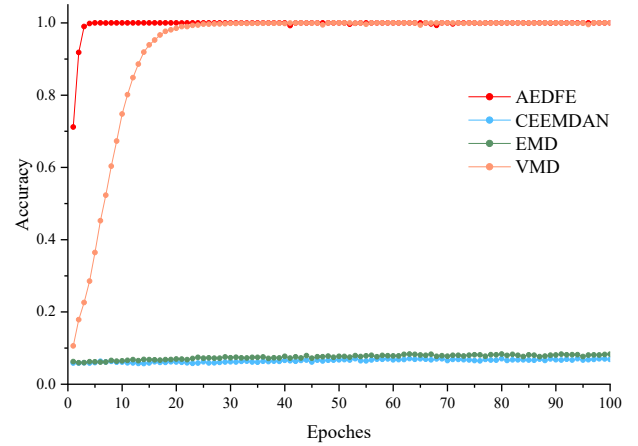


Fig. 18. Test accuracy plot of the model during the training process with 70% of the data as input for the four different methods

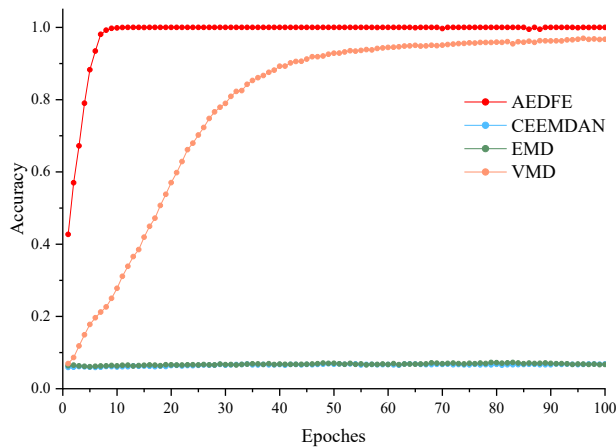


Fig. 16. Test accuracy plot of the model during the training process with 30% of the data as input for the four different methods.

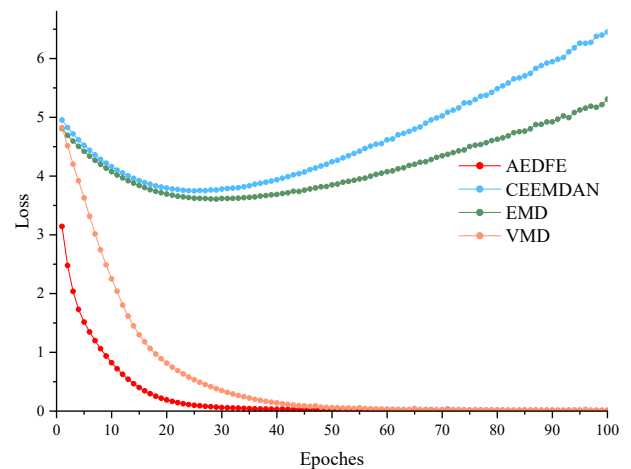


Fig. 19. Test loss plot of the model during the training process with 70% of the data as input for the four different methods.

During the model training process, the t-SNE (t-distributed Stochastic Neighbor Embedding) technique was applied to project feature images into a two-dimensional space to visualize the evolution of feature clustering across different convolutional layers. Fig.20 presents the visualization results of this process. At the initial stage of the model, the distribution of feature images is relatively chaotic, indicating a high degree of feature dispersion. However, as the convolutional layers progressively process the features, the extraction and aggregation of features lead to a more uniform distribution, and the clustering situation significantly improves. This result indicates that the convolutional layers play an important role in extracting fault features, making the feature representation more concentrated and clearer.

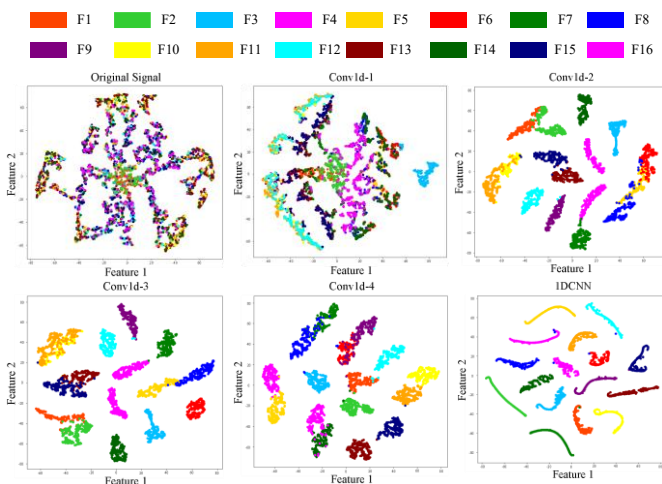


Fig. 20. t-SNE Feature Visualization.

By employing AEDFE for feature extraction, the diagnostic model achieved a perfect training accuracy of 100.00% and a validation accuracy of 99.98%, demonstrating superior generalization performance. Compared with the other three feature extraction methods, the proposed approach exhibited a significant improvement in validation accuracy, particularly

under small-sample conditions. The competing methods suffered from severe overfitting due to limited training data, leading to a sharp decline in testing accuracy. In contrast, our method maintained high accuracy in both training and testing phases, even in noisy and small-sample scenarios, highlighting its robustness.

## 6. Conclusion

In modern DC-DC converter fault diagnosis, accurately identifying parametric faults is crucial for ensuring device reliability and performance. However, existing feature extraction methods often face insufficient extraction capabilities in strong noise environments and small sample sizes, which negatively impacts diagnostic accuracy. To address this challenge, this study proposes an innovative AEDFE method. This approach effectively enhances the differentiation between features of various parametric faults by accurately extracting spatial characteristics from fault signals, significantly improving diagnostic accuracy.

Experimental results demonstrate that the proposed AEDFE method achieves perfect fault diagnosis accuracy (100%) even in strong noise environments, outperforming the three baseline methods by an average margin of 61.61%. Notably, when the training data size is reduced to only 10% of the original dataset, AEDFE still maintains a near-perfect accuracy of 99.98%, surpassing the comparative methods by 77.64%. These findings not only confirm AEDFE's exceptional noise immunity but also demonstrate its remarkable robustness in data-scarce scenarios. Consequently, AEDFE offers a highly reliable and efficient solution for high-precision fault diagnosis in DC-DC converters, showcasing substantial practical value and broad application potential in industrial settings.

## References

1. Hao Z ,Han R ,ChuanZhi Y , et al. Ripple-based matrix modeling and cross-coupling effect analysis of double-input DC-DC Boost converters.Sci. China Technol. Sci. vol.65, no.8, pp.1878-1890. <https://doi.org/10.1007/s11431-021-1979-3>
2. Khan Shahamat Shahzad;Wen Huiqing. A Comprehensive Review of Fault Diagnosis and Tolerant Control in DC-DC Converters for DC Microgrids. IEEE Access, vol.9, pp.80100-80127, <https://doi.org/10.1109/ACCESS.2021.3083721>.
3. Mejia-Ruiz E G ,Paternina A R M ,R. R R J , et al. A System Identification-based Modeling Framework of Bidirectional DC-DC Converters for Power Grids. Journal of Modern Power Systems and Clean Energy, vol.10, no.3, pp.788-799, May. 2022. <https://doi.org/10.35833/MPCE.2020.000836>.
4. G. Zhang and J. Yu,. Open-circuit fault diagnosis for cascaded H-bridge multilevel inverter based on LS-PWM technique. CPSS Transactions on Power Electronics and Applications, vol.6, no.3, pp.201-208, Sept. 2021.

<https://doi.org/10.24295/CPSSTPEA.2021.00018>.

5. Sun, Y., Du, W., Gui, L., Duan, X., & Hao, L. Design of magnetic pole detection coils for open-circuit and short-circuit fault detection in multiphase brushless excitation machines. *Transactions of China Electrotechnical Society*, vol.37, no.14, pp.3542-3554, <https://doi.org/10.19595/j.cnki.1000-6753.tces.210199>.
6. Kong X ,Zhan M ,Lin H , et al. Time-varying characteristics of acoustic emission and fractals based on information dimension during structural failure of coal subjected to uniaxial compression. *Measurement*, vol.236, <https://doi.org/10.1016/j.measurement.2024.115088>.
7. W. -C. Wang, L. Kou, Q. -D. Yuan, J. -N. Zhou, C. Liu and G. -W. Cai, An Intelligent Fault Diagnosis Method for Open-Circuit Faults in Power-Electronics Energy Conversion System. *IEEE Access*, vol.8, pp.221039-221050, <https://doi.org/10.1109/ACCESS.2020.3043796>.
8. S. Zhuo, A. Gaillard, L. Xu, C. Liu, D. Paire and F. Gao, An Observer-Based Switch Open-Circuit Fault Diagnosis of DC - DC Converter for Fuel Cell Application. *IEEE Transactions on Industry Applications*, vol.56, no.3, pp.3159-3167, <https://doi.org/10.1109/TIA.2020.2978752>.
9. M. Terasaki, Y. Oohashi, Y. Masuyama and T. Sudo, Design and analysis for noise suppression of DC/DC converter. 2014 IEEE Electrical Design of Advanced Packaging & Systems Symposium (EDAPS), Bangalore, India, 2014, pp.109-112, <https://doi.org/10.1109/EDAPS.2014.7030827>.
10. L. Xie, X. Ruan, H. Zhu and Y. -K. Lo, Common-Mode Voltage Cancellation for Reducing the Common-Mode Noise in DC - DC Converters. *IEEE Transactions on Industrial Electronics*, vol.68, no.5, pp.3887-3897, <https://doi.org/10.1109/TIE.2020.2984438>.
11. Liang, H., Cao, J., & Zhao, X. Small sample fault diagnosis method for rotating machinery based on GADF and PAM-ResNet. *Control and Decision*, vol.38, no.12 pp.3465-3472, <https://doi.org/10.13195/j.kzyjc.2022.0378>.
12. Lei Y, Yang B, Jiang X, Jia F, Li N, Asoke K. Nandi, Applications of machine learning to machine fault diagnosis: A review and roadmap. *Mechanical Systems and Signal Processing*, vol.138, <https://doi.org/10.1016/j.ymsp.2019.106587>.
13. Jiang, H., Shang, C., & Gao, R. Research on fault noise diagnosis and recognition method for wheel-rail based on EMD and neural networks. *Vibration and Shock*, vol.33, no.17, pp.34-38, <https://doi.org/10.13465/j.cnki.jvs.2014.17.007>.
14. Li, R., & Fan, Y. Fault diagnosis of unidirectional valves in high-pressure diaphragm pumps based on CEEMDAN multi-scale permutation entropy and SO-RELM. *Vibration and Shock*, vol.42, no.05, pp.127-135, <https://doi.org/10.13465/j.cnki.jvs.2023.05.016>.
15. Sudhar R ,Jaskaran S ,Ashish P. VMD-Based Ensembled SMOTEBoost for Imbalanced Multi-class Rotor Mass Imbalance Fault Detection and Diagnosis Under Industrial Noise. *Journal of Vibration Engineering & Technologies*, vol.12, no.2, pp.1457-1478, <https://doi.org/10.1007/s42417-023-00920-w>.
16. Wen, S., Ma, Y., & Sun, Z. Short-term power prediction of photovoltaic generation based on GWO-EEMD-BP neural network. *Journal of Central South University (Science and Technology Edition)*, vol.53, no.12, pp.4799-4808. 2022.
17. Wu, J., Li, M., & Tang, W. Fault diagnosis of industrial circulating water system supply pumps based on DTCNN-SVM. *Vibration and Shock*, vol.42, no.13, pp.226-234, <https://doi.org/10.13465/j.cnki.jvs.2023.13.027>.
18. Liu Y ,Zhang R ,He Z , et al. The study of hydraulic machinery condition monitoring based on anomaly detection and fault diagnosis. *Measurement*, vol.230, <https://doi.org/10.1016/j.measurement.2024.114518>.
19. Wang, Y., Li, W., Zhao, H., et al. Transformer fault diagnosis method based on dissolved gas analysis in oil using DBN-SSAELM. *Power System Protection and Control*, vol.51, no.04, pp.32-42, <https://doi.org/10.19783/j.cnki.pspc.220662>.
20. Zhang, S., Ji, H., & Liu, Y. Bearing fault diagnosis based on ISCNN-LightGBM. *Control Theory and Applications*, vol.40, no.04, pp.753-760. 2023.
21. X. Zhang, P. Han, L. Xu, F. Zhang, Y. Wang and L. Gao, Research on Bearing Fault Diagnosis of Wind Turbine Gearbox Based on 1DCNN-PSO-SVM. *IEEE Access*, vol.8, pp.192248-192258, <https://doi.org/10.1109/ACCESS.2020.3032719>.
22. Cui, G., Zhong, Q., Zheng, S., et al. Multi-sensor fusion bearing fault diagnosis based on VMD grayscale image encoding and CNN. *Vibration and Shock*, vol.42, no.21, pp.316-326, <https://doi.org/10.13465/j.cnki.jvs.2023.03.020>.
23. Chang, C., Mei, J., Zhao, H., et al. Fault diagnosis of high-pressure oil circuits in diesel engines based on CUM3-CNN. *Vibration and Shock*, vol.42, no.03, pp.174-180, <https://doi.org/10.13465/j.cnki.jvs.2023.03.020>.
24. Cao, J., Yin, H., & Wang, J. Generator bearing fault diagnosis method based on MACDCGAN. *Vibration and Shock*, vol.43, no.11, pp.227-235, <https://doi.org/10.13465/j.cnki.jvs.2024.11.025>.